CHAPTER 5: CHARACTERIZATION OF THE BACKFILL SOIL

5.1 INTRODUCTION

The backfill in the pipe-soil box tests was dry and was mostly comprised of quartz sand. Tests were performed to characterise the soil. The tests ranged from basic index tests to engineering strength tests (a range of triaxial tests). The objective of the triaxial testing was to define the critical state line for the soil and to determine a relationship between state parameter, current strength and dilation. Ultimately this will allow determination of an appropriate constitutive relationship for the soil. Numerical modelling can then be undertaken of the boundary value problem involving the interaction between soil and pipe in a trench as the surface of the backfill is loaded.

Most of the engineering strength tests were conducted on samples compacted to a medium dense state, reflecting the general level of compaction achieved with the backfill in the pipe-soil box tests.

5.2 DEFINITION OF THE BACKFILL MATERIAL

All tests on the soil described in this section, were generally conducted at the laboratories of the Centre for Geotechnical Research in the University of Sydney and in accordance with Standards Australia, AS1289, wherever applicable.

The sand used in the tests was a commercially available sand from Adelaide used for concrete mixing, which was largely comprised of crusher waste from a quartzite quarry. Particle size distribution curves for the soil are given in Figure 5-1. Each curve represents the average of five sieve analyses for a triaxial test specimen, prior to testing. The average of the two curves is presented in Figure 5-2. In this same Figure, particle size distributions have been imposed for the soil after triaxial testing. The maximum mean stress levels in the two tests were 0.5 and 1.4 MPa for tests DAC001 and DAC004, respectively. Given the natural variability of the particle size

distribution for the sand evident in Figure 5-1, there was no discernible shift in the position of the curve after stressing the soil to 1.4 MPa, indicating the soil had not suffered any significant crushing during triaxial testing.

The sand was poorly graded and would be classified as SP in the Unified Soil Classification System. Table 5-I provides parameters derived from the particle size distribution of the soil.

The particle density was 2.66 t/m^3 (to AS1289 C5.1) and the maximum and minimum dry densities (to AS1289 E5.1) were 1.75 and 1.405 t/m^3, respectively. Accordingly the maximum and minimum void ratios were 0.893 and 0.520, respectively.

The sand was angular as seen in the scanning electron microscope images of four samples in Figure 5-3. A thin section of the sand was prepared and it was determined that it was composed of 97% quartz, 1% muscovite, 1% feldspar and 1% tourmaline and iron oxides. The parent rock was assessed independently to be a metamorphic quartzite.

5.3 SOIL TESTS DURING THE PIPE TEST SERIES

For construction control during the pipe tests, correlations were developed between density index and the resistance to penetration of a falling weight penetrometer (Scala Penetrometer, to AS 1289 F3.2 – 1984). Tests were conducted by compacting the dry sand in a steel drum (a 44 gallon drum, 565 mm in diameter) to a wide range of densities (I_D = 50 to 85%). Subsequently the penetration test was performed on each preparation. The average density of the sand was determined after compaction of the soil by weighing the drum and its contents.

A linear relationship was evident between penetration resistance (blows / 300 mm of penetration) and density index for reasonably dense sand, with an increase of the blowcount by one being caused by an increase of density index of approximately 4.5%. At lower levels of density, the penetrometer was unable to discern the density

index as the self-weight of the device was all that was needed to penetrate the soil. Therefore inferred density indices for penetration resistances less than 1.5 blows per 300 mm of penetration should be treated cautiously. Fortunately this limit was breached in only one pipe installation (P375/1, in which 1 blow / 300 mm was recorded).

It should also be noted that small shifts were apparent in the correlation between blow count and sand density for the different batches of sand.

An estimate of Young's modulus of the backfill sand was required for the design of the earth pressure cells, which were used in a number of the buried pipe tests. The 44 gallon drum was again employed. Sand was compacted in the drum to a height of 750 mm, and the density of the sand was checked. Then a plate loading test was conducted with a rigid steel plate, 270 mm in diameter. During loading of the plate, settlement was measured using three dial gauges secured to a reference beam.

A graph of applied pressure against plate settlement was obtained (Figure 5-4). Apart from an initial settling in, the relationship between settlement and pressure appeared to be linear to 450 kPa in the two tests that were conducted. The slopes of the lines for the two tests were almost identical, which was to be expected as the estimated average density index of the soils was 75% ± 2 below a depth of 0.35 m. The slope enabled the estimation of the average elastic modulus of the sand, assuming purely elastic behaviour and ignoring the restraint afforded by the steel drum. The drum had a diameter 2.1 times that of the loading plate. Adopting a Poisson's Ratio of 0.3, Young's modulus was estimated to be 10 MPa.

5.4 THE TRIAXIAL TESTING PROGRAM

The purpose of the triaxial tests was to define the Critical State Line for the soil. Five constant mean stress tests, five constant volume tests and three conventional drained triaxial tests were conducted in an attempt to approach the CSL from different directions. Shearing the samples to large strains was essential for

meaningful interpretation of the critical state line. As the buried pipe tests were conducted in dry sand, the triaxial tests were performed also on dry soil samples.

5.4.1 Triaxial Testing Procedures

Samples were set up at the desired dry density by placing a split tube former over the bottom pedestal as indicated in Figures 5-5a and 5-5b. The former was clamped firmly together for sample preparation. The space between the former and the fitted membrane was evacuated with a small vacuum pressure (≈ 10 kPa) to ensure that the membrane did not interfere with the compaction process. The soil was placed in layers, which were rodded as uniformly as possible to achieve the desired sample height. Care was taken in the placement of the final layers to ensure that the vacuum was effective in restraining the membrane. Otherwise a local reduction of diameter or 'necking' could occur.

After compaction, the top cap or platen was gently tamped into position and the membrane was secured to it with two O-rings. The membrane was rolled over the bottom pedestal and a vacuum pressure of 10 to 15 kPa was transferred to the sample through the drainage port. O-rings were placed over the bottom pedestal after the former was removed. An example of the excellent dimensional control of the dry sand specimens is provided in Figure 5-5c.

Conventional platens were used. Lubricated, over-sized platens have been advocated by a number of authors to ensure uniform sample stresses (e.g. Lo and Lee, 1990), but this equipment and the techniques for its application were not available. A particular problem with such platens is the fitting of a membrane to the sample. Moreover, the need for frictionless platens is diminished as the length to diameter ratio of the sample approaches two or greater (Bishop and Green, 1965). The samples in this test series had a length to diameter ratio of 1.9.

A disc of filter material was placed on the base pedestal to prevent intrusion of fine soil particles into the drainage port. The fine filter may have reduced the frictional resistance to an extent at the soil - platen interface.

The cell was then filled with water and a cell pressure slightly greater than the temporary vacuum pressure was applied. The vacuum pressure was then removed and the base drainage port was left open to allow release of air from the dry sample. Minor settlement of the sample may have occurred during this set-up period as a small, isotropic pre-consolidation pressure of a maximum of 30 kPa was applied to the sample for a short period as the sample former and vacuum pressure were removed.

Care was taken to establish the initial density of each specimen. The diameter of the sample was taken to be the diameter of the split former less two thicknesses of the rubber membrane. A membrane thickness of 0.35mm was found to be the practical minimum thickness for this soil to ensure leaks did not occur at the large sample strains attained in the tests. The height of the sample was measured with the top platen in position. All samples were approximately 100 mm in diameter and 190 mm long. The mass of the sample was established by weighing a chosen mass of the dry soil used to form the sample, and then deducting the mass of soil remaining after preparation of the sample. The final sample mass was measured by carefully collecting the soil at the end of the test. Inevitably, some grains of the dry sand were lost in this final operation.

Table 5-II provides a summary of the 13 tests that were conducted and the initial sample parameters. Most samples were prepared to a medium dense state with density indices in the range from 50 to 70% after the initial isotropic consolidation stage. Two constant volume test samples, DAC004 and CVT2/95, had density indices outside this range and were relatively dense and loose, respectively.

All samples were isotropically consolidated before commencing the main test by ramping the cell pressure at a rate of 2.5kPa / minute. The initial settlement due to consolidation was relatively small and was assumed to be isotropic.

During testing, volume changes were estimated from cell fluid volume changes, which were measured by a GDS hydraulic ram system. Volumes were corrected for cell volume changes (expansion or contraction) with cell pressure. Corrections were also made for the penetration of the loading ram. The dependence of cell volume on

cell pressure was established by placing a steel cylinder of similar dimensions to a soil sample in the cell, applying a cell pressure and recording the change in volume of the cell fluid on the GDS device. The cell fluid volume stabilised after approximately ten minutes, depending on the level of cell pressure increment. De-aired, de-mineralized water was used for the cell fluid. It was found that some air still existed in the water after 'de-airing' and it was essential to carry out a number of cell calibration runs before the calibration settled down. With air in the system, cell volume changes are greater than the apparent measurement, as air is forced into solution.

Axial strains were measured electronically outside the cell, while axial load was measured inside the cell. Calibrations of both displacement and load transducers were performed prior to each test series.

The maximum axial strain rate in all the tests was 0.05 mm/minute. Wherever possible, axial strains were taken above 25%.

Sample length and volume changes were used to derive the average area of the sample during testing to determine the deviator stress, q.

5.5 RESULTS OF THE TRIAXIAL TESTS

Generally sample strains at the end of testing exceeded 20%, except for two early constant volume tests, DAC001 and DAC002, which were concluded before 15% had been reached. Samples were noticeably barrelled at the end of testing as indicated in the photographs in Figure 5-6. Membrane breakages were rare, but did occur, curtailing one or two of the triaxial tests. Tilting of the top platen was observed occasionally towards the end of testing.

Membrane stress corrections were considered when reducing the triaxial test data, based on hoop stress theory (Ooi, 1990). Assuming a modulus of 1.2 MPa for the latex membrane and a thickness of 0.35 mm, the maximum correction was 1.5 kPa and so it was decided that at this low level the correction could safely be ignored.

The following section provides data on the sand relating to the properties:

- Initial compressibility under isotropic loading (consolidation stage)
- Soil stiffness
- Post-peak behaviour
- Shear strength
- Constant volume shear strength
- Dilation

A summary of the major findings is given at the end of the Chapter.

5.5.1 Soil Compressibility in the Isotropic Consolidation Stage

The isotropic consolidation stage of the triaxial tests provided information on the initial compressibility of the soil over a range of densities and mean stresses (refer Figure 5-7). Four of the triaxial tests were not included in the plot, because of the small change of the cell confining pressure in the initial consolidation phase for these tests.

A compression index could be discerned for each of the samples, which was reasonably constant over a designated mean stress range. In some cases where the stress levels were high, two indices have been reported for the one test, corresponding to different stress ranges. The initial compression indices, C, for the samples have been presented in Table 5-III, with C being defined as:

$$C = -\frac{\Delta e}{\Delta(\ln p')} \qquad 5\text{-}1$$

An examination of the data in Table 5-III revealed that the compressibility increased with the average of the mean stress range and was little influenced by the variations in density index of the samples.

5.5.2 Stress-Strain Data

Figure 5-8 provides the relationships measured in the experiments between the stress ratio, q/p′, and axial strain for the various test series. As the numerical modelling required a convenient form with which to express the stiffness of the soil and its variation with stress, the triaxial tests were interpreted to give moduli, E. For

simplicity, it was decided to determine secant values rather than a tangent moduli. Tangent moduli can be determined from secant values as expained later. The stress level at which the secant modulus was determined was $0.5q/p'_{max}$.

The data for the moduli have been presented in Table 5-IV. The mean pressures and corresponding secant moduli at 50% of q/p'_{max} were normalised with respect to atmospheric pressure, p_a, and then plotted to establish a power relationship similar to that advocated by Janbu (1963), i.e.

$$E = mp_a\left[\frac{p'}{p_a}\right]^{(1-a)} \qquad 5\text{-}2$$

Figure 5-9 provides the secant modulus data and includes a line of best fit, which was given by:

$$E = 178p_a\left[\frac{p'}{p_a}\right]^{(1-0.42)} = 178p_a\left[\frac{p'}{p_a}\right]^{0.58} \qquad 5\text{-}3$$

The statistical coefficient of determination for the data, r^2, was 0.82.

The exponent agrees well with the findings of Janbu for sand. According to Figure 3-1, the coefficient, a, has a value of 0.42 at a porosity between 35 and 50%. The void ratio and hence porosity of the sand (e/(1+e)) varied throughout the test series as indicated in Table 5-II. The porosity ranged between 37 and 44%, and the average porosity for all the tests was 40%, well within the range of Janbu's data.

5.5.3 Shear Strength of the Sand

The strength of the soil and the contribution of dilation were determined from the triaxial testing program. The three conventional triaxial tests (CID, consolidated isotropically, then sheared in the drained state) gave an average peak friction angle, ϕ'_{max}, of 37°, while the corresponding value for the constant mean stress tests was 38°. The peak friction angles for individual tests are given in Table 5-V and the

variation of this strength parameter with initial sample density over all the tests is given in Figure 5-10.

The peak friction angle increased almost linearly with density index. The relationship could be approximated by the expression;

$$\phi'_{max} = 0.104I_D + 30.6 \qquad 5\text{-}4$$

where, ϕ'_{max} is in degrees and I_D is in %.

The critical state strength (ϕ'_{cv}) was evaluated from the stress conditions at the end of testing. The accuracy of such an approach depends on whether or not critical state had been reached. In section B.1 of Appendix B, the rate of volume strain with axial strain has been imposed on the stress-strain plots for each of the tests. It can be seen that the rate of volume strain had slowed by the end of each test, but it could not be said that it had stopped, despite the large shear strains developed in the tests. Therefore the estimate of ϕ'_{cv} will be on the high side.

Furthermore the accuracy of this estimate will depend on whether a general failure had developed throughout each sample or shear banding had dominated the soil behaviour. In the latter case, the critical state may only prevail in the locality of the shear band.

The data have been plotted in Figure 5-11 and it can be seen that the data are bounded by values of 33° and 31.5°. One point (DAC004) has been omitted from this Figure for the purpose of clarity, as the stresses associated with it were much higher than for any other test. DAC004 plotted almost on the 33° line. The stress-strain (q/p against ε_a) plots for each test series in Figure 5-8 have had two potential values of the critical state stress ratio, M, imposed upon them for ϕ'_{cv} values of 31.5° and 29°. The corresponding values of M are 1.27 and 1.16. The latter estimate will be discussed in the next section. It is evident from Figure 5-8 that a value of ϕ' of 31.5° forms a reasonable lower bound to the test data.

Referring to equation 5-4, a further estimate of ϕ'_{cv} is provide by the constant of 30.6, which is equivalent to the friction angle at a density index of zero in degrees. This value is almost one degree less than the value derived from the end of test data. However this value relies on extrapolation of an assumed linear relationship between ϕ'_{max} and I_D.

5.5.4 The Critical State Line

By plotting the end points of the three series of tests on a plot of void ratio, e, against the natural logarithm of the effective mean stress, ln p′, an approximation to the critical state line may be made, assuming that critical state has been reached. The constant volume tests are presented in Figure 5-12. It is clear from this plot that the first three tests were not truly constant volume tests; a small error in the algorithm for volume control was found subsequently and corrected. Furthermore, tests DAC001 and DAC004 were ended at relatively low levels of axial strain and were unlikely to have been close to critical state.

A suggested critical state line is indicated on the Figure, which is defined by an intercept on the void ratio axis, Γ, of 1.07 at a reference effective mean stress, p′, of 1 kPa, and a gradient, λ, of 0.055. The end point for DAC004 is furthest removed from the line, which is most probably due to the early termination of the test and the high level of mean stress reached in this test (approximately 1400 kPa). Some particle breakage may have occurred at this stress level, which would shift the critical state line, increasing the magnitude of its gradient, as observed by Been, Jefferies, and Hachey (1991) and Ajalloeian and Yu (1996).

The two remaining test series have been plotted similarly in Figures 5-13 and 5-14, and a critical state line has been judged for each series. A statistical fit was not deemed appropriate for the data. The variation of the critical state line parameters for the three test series is provided in Table 5-VII. The three conventional triaxial tests provided a state line with a relatively low gradient, indicating less compressible soil.

End points for all tests have been plotted in Figure 5-15 and the estimates of the CSL have been drawn over the data. It can be seen that the "constant volume" tests generally reached higher void ratios by the conclusion of testing for a given stress level than either the CID or constant mean stress tests. The latter two series of tests reached similar levels of void ratio and a single critical state line defined by $\Gamma = 0.99$ and $\lambda = 0.05$ would seem reasonable for these tests.

The adopted critical state line for the sand from the constant volume tests, has been compared with others reported in the literature in Figure 5-16 (the adopted CSL is denoted as "DAC sand"). The adopted CSL was defined by Γ of 1.07 and λ of 0.055. Both the gradient and the intercept at the reference pressure of 1 kPa were outside the bounds of the published data; the gradient was relatively high, indicating significantly more compressible sand. The intercept was similar to that for Reid-Bedford sand, however the gradients differed by a factor of 2. Reid Bedford sand has been described as sub-angular, while the sand in the current study was angular. The difference in the maximum and minimum void ratios was greater (16%) than Reid Bedford sand, and the uniformity coefficient of 2.6 compared with a value of 1.6, indicating that "DAC sand" was more poorly graded.

Hokksund sand has been reported as sub-angular sand, with similar properties to DAC sand. The major difference was the basic particle size ($D_{10} = 0.21$, while for DAC sand it was 0.16), which may be responsible for the relatively low compressibility of the soil.

Knowing the critical state line, which as previously stated was based on the CSL from the constant volume tests, and adopting a critical state strength of ϕ'_{cv} of 31.5°, the difference between the peak and critical state friction angles may be plotted against the state parameter at $(q/p')_{max}$. The strength and dilation data from Table 5-V were used for this Figure. The data have been plotted in Figures 5-17 and 5-18.

The data fit centrally within the bounds proposed by Been and Jefferies in 1985 (refer Figures 3-16 and 5-17). If either the CSL from the CID or constant mean stress tests are applied, the data points tend to plot on the upper bound line proposed

by Been and Jefferies. By definition, a soil at critical state has a state parameter of zero and ϕ'_{max} should equal ϕ'_{cv}. Therefore sands would be expected to pass through the origin, close to the lower bound proposed by Been and Jefferies. The data in Figure 5-17 indicate however, that a difference in the friction angles of almost 2° could be expected at the critical state. The other two experimentally derived CSL's would suggest twice this value and are therefore considered to be less reliable. The offset at a state parameter of zero may in part be due to overestimation of the critical state strength.

The data in Figure 5-17 has been re-plotted in Figure 5-18 to evaluate the coefficient, A, in the expression;

$$(\phi' - \phi_{cv}') \text{ radians} = A(e^{-\xi} - 1) \qquad 5\text{-}5$$

For the sand in this study the line of best fit to the data was given by:

$$(\phi' - \phi_{cv}') \text{ radians} = 0.66(e^{-\xi} - 1) + 0.034 \qquad [r^2 = 0.80] \qquad 5\text{-}6$$

Enforcing the statistical trend line through zero gave the expression:

$$(\phi' - \phi_{cv}') \text{ radians} = 0.98(e^{-\xi} - 1) \qquad [r^2 = 0.58] \qquad 5\text{-}7$$

The two lines given by these equations have been superimposed on the data in Figure 5-18, the broken line corresponding to equation 5-6 and the solid line corresponding to 5-7. It is evident that the relationship expressed by 5-7 is unsatisfactory, as it will overestimate ϕ' at low values of state parameter and underestimate at high values.

A much simpler expression could be adopted based on a linear relationship between the strength difference and state parameter:

$$(\phi' - \phi_{cv}') \text{ degrees} = -41.5\xi + 1.8 \qquad [r^2 = 0.80] \qquad 5\text{-}8$$

Enforcing the statistical trend line through zero altered the expression to:

$$(\phi' - \phi_{cv}') \text{ degrees} = -59.6\xi \qquad [r^2 = 0.62] \qquad 5\text{-}9$$

Alternatively, a parabolic relationship may better express the apparent non-linear link between $(\phi' - \phi'_{cv})$ and state parameter:

$$(\phi' - \phi'_{cv}) \text{ degrees} = -331\xi^2 - 96.8\xi \qquad [r^2 = 0.80] \qquad 5\text{-}10$$

This non-linear equation has the advantages that it enforces zero dilation once the state parameter increases to zero and follows the data satisfactorily for this sand. However the fit for the parabola is no better statistically than that for the linear relationship of equation 5-8. The parabolic equation suggests that dilation may slow at low values of state parameter. This feature of the correlation appears to be at odds with the findings of Been and Jefferies.

All the expressions based on state parameter, which are represented by equations 5-8, 9 and 10, are compared with the data in Figure 5-19. The statistical fit is significantly weakened by enforcing the critical state strength at critical state, or a value of state parameter of zero. Equation 5-9 would appear to be the most acceptable expression, both theoretically and experimentally for the range of state parameters encountered in the laboratory test series, although it is not a statistically strong relationship.

5.5.5 Dilational Behaviour of the Sand

As discussed in Chapter 3, Bolton (1986) defined dilation in terms of total strains, i.e. equation 3-24:

$$D_B = -\frac{d\varepsilon_v}{d\varepsilon_1}$$

According to Bolton, a sample undergoing triaxial stresses would experience a maximum dilation rate corresponding to its dilatancy index, I_R. The dilatancy index is a function of the effective mean stress and the density index of the soil.

The density index of the sand at peak strength provided values of I_R, which gave better correlations with soil parameters than the initial density index at set-up of the soil sample. All values of Bolton's dilatancy index subsequently referred to in this thesis have been calculated using the density index at peak strength.

It was discovered that Bolton's estimate of maximum dilation was reasonable provided the material constant, Q, was 9, not 10 as in Bolton's original formulation (equation 3-26), although he had anticipated lower values of Q for weaker grained soils. Material constant, R, remained at unity. Therefore the sand in this study has a dilation index best expressed by:

$$I_R = I_D(9 - \ln p') - 1 \qquad 5\text{-}11$$

The maximum value of Bolton's dilation for each of the triaxial tests has been plotted in Figure 5-20 against I_R, as determined by eqn 5-11. The density index at maximum stress ratio has been adopted to generate values of I_R. In the same Figure, the maximum dilation has been plotted against state parameter at maximum stress ratio. It would appear that state parameter is a slightly better indicator of dilation.

The similarity of the two plots suggested a strong relationship between state parameter and dilatancy index, as one would expect with both indices being functions of effective mean stress and void ratio. When plotted against one another (Figure 5-21), it was found that dilation index was reliably given by:

$$I_R = -10.7\xi \qquad [r^2 = 0.94] \qquad 5\text{-}12$$

This equation is represented by the trend line to the data in Figure 5-21. A slightly better correlation is possible if a zero offset is accepted.

Bolton's recommendation of $D_{Bmax} = 0.3I_R$ may then be replaced by:

$$D_{Bmax} = -3.20\xi \qquad 5\text{-}13$$

This relationship appears as a straight line on the plot of dilation against state parameter in Figure 5-20.

Bolton (1986) suggested that the maximum dilation under triaxial conditions may be found from the dilatancy index according to equation 3-28:

$$(\phi'_{max} - \phi'_{cv}) = 3I_R°$$

However it was found that with the value of Q adopted in this study and the application of the density index at peak strength to derive I_R, the above equation significantly underestimated dilation. The plot in Figure 5-22 of the difference in the two angles of friction against dilatancy index revealed that at least $6I_R$ would be needed to approach the levels of dilation realised in this test series. Combining equations 5-9 and 5-12 provided the following outcome;

$$(\phi'_{max} - \phi'_{cv}) = 5.57I_R° \qquad 5\text{-}14$$

Interestingly, Bolton recommended a value of $5I_R°$ for plane strain conditions. So it may be concluded that for this sand, Bolton's equation for plane strain is a better approximation to the triaxial compression data than his recommendation for triaxial strain.

The curved line in Figure 5-22 has been produced by combining equations 5-10 and 5-12, resulting in a non-linear relationship between the friction angle difference and Bolton's dilatancy index, i.e.:

$$(\phi'_{max} - \phi'_{cv}) = -2.89I_R^2 + 9.05I_R \qquad 5\text{-}15$$

The Davis flow rule, which was extended to triaxial compression of frictional soils by Carter, Booker and Yeung (1986), was applied to the test data to derive estimates of the maximum dilation angle, Ψ_{max}. This estimate was then plotted against the experimental data of $(\phi'_{max} - \phi'_{cv})$, Bolton's index, I_R and state parameter, ξ, in Figures 5-23, 24 and 25, respectively.

The "Davis" dilation angle is not strongly correlated with difference in effective friction angle (Figure 5-23). Bolton's recommendation for plane strain, that (ϕ'_{max} - ϕ'_{cv}) equals 0.8ψ, is indicated in the Figure. This relationship has been applied to triaxial conditions by other researchers. Although the straight line though the origin expressed by Bolton's relationship passes through the data, the correlation coefficient was only 0.14.

Better correlations are evident in Figures 5-25 and 5-26 between either Bolton's dilation index, I_R, or state parameter, ξ, and the maximum dilation angle. Correlation coefficients of 0.80 and 0.85 were found for linear relationships between the estimated dilation angle and I_R and ξ, respectively. The relationships were:

$$\psi_D = 7.09 I_R \qquad 5\text{-}16$$

$$\psi_D = -75.2\xi \qquad 5\text{-}17$$

The notation, ψ_D, in the above expressions indicates that the dilation angle has not been measured, but has been calculated on the basis of the Davis flow rule. The units of ψ_D in the equations above are degrees.

The last equation is attractive in its simplicity, particularly for numerical modelling, and suggests that state parameter and the Davis flow rule may provide the basis of a powerful model for the stress-deformation behaviour of the sand.

Rowe's stress-dilatancy expression (equation 3-22) was compared also with the triaxial test data in Figure 5-26. Bolton's dilation term, D_B, the ratio of total volumetric to total axial strain, was derived from Rowe's expression for two assumed values of ϕ'_f, 31.5° (the adopted value of ϕ'_{cv} for the sand) and 30°. In the plot of D_B against ϕ'_{max}, the stress –dilatancy expression is seen to provide two curves for each of the ϕ'_f values. The test data points are aligned reasonably well with the 31.5° curve, although the dilation for two tests were significantly underestimated; tests CONP100 and 53TRDAC were both medium dense sand preparations, which were tested under initially low confining pressures.

Manzari and Dafalias (1997) suggested that the stress ratio at the onset of dilation, M_c^d was needed to adequately predict dilation (refer Chapter 3, equation 3-46). The authors contended that M_c^d was a function of state parameter (refer equation 3-47), with $\left(M_c - M_c^d\right)$ being directly proportional to state prameter, ξ.

Data concerning the onset of dilation from the triaxial tests has been summarised in Table 5-VII. e_c^d is the void ratio at the onset of dilation. The state parameter was evaluated for this void ratio and the effective mean stress by adopting Γ of 1.07 and λ of 0.055.

Combining the data in Tables 5-V and 5-VII leads to the plots of $\left(M_c - M_c^d\right)$ against state parameter in Figure 5-27, and dilation against $\left(M_c^d - \eta_{max}\right)$ in Figure 5-28. M_c was based on a ϕ'_{cv} value of 31.5°. The dilation in Figure 5-28 is the maximum "total" dilation, defined by the ratio of total volumetric strain to total shear strain.

It is evident that there is not a strong correlation between $\left(M_c - M_c^d\right)$ and state parameter, thereby diminishing the usefulness of Manzari and Dafalias' model for this sand. However their flow rule is supported reasonably well by the test data in Figure 5-28, despite the use of total strains to define dilation. Again the correlation as illustrated by the dashed trendline is weak (r^2 = -0.2), caused largely by four outlying points. The trendline in the Figure has a gradient of 0.73, giving a value of 0.90 for the Manzari and Dafalias' coefficient, A, in equation 3-46.

5.6 SUMMARY OF THE CHAPTER

The sand in the study was a poorly graded sand formed by crushing of quartzite. Consequently the sand grains were angular and mica and feldspar particles were present.

Three series of triaxial tests were performed on the dry sand, which had been prepared at a range of densities (I_D approximately 30 to 80%). The tests included consolidated isotropically, conventional drained triaxial tests (CID), constant volume and constant mean stress tests. A major aim of the triaxial tests was to induce large axial strains so that information about the critical state of the sand could be obtained.

The major findings of this limited experimental study were;

(i) The initial compressibility of the sand under isotropic loading was low.

(ii) Shearing of the soil to large strain produced strain softening and associated dilation.

(iii) The secant modulus of the soil at 50% peak stress ratio could be reasonably well represented by a power relationship with effective mean pressure as proposed by Janbu (1963) and, significantly, the coefficients in the relationship agreed with Janbu's recommended values.

(iv) The peak shear strength of the sand in the various tests was found to vary in direct proportion to the initial sample density index.

(v) The critical state shear strength, ϕ'_{cv}, was estimated to be 31.5°.

(vi) The critical state line varied slightly between the different types of tests, with the constant volume tests providing a "higher" CSL, defined by values of Γ of 1.07 and λ of 0.055. This was the chosen CSL as it gave a lower positive value of $(\phi'-\phi'_{cv})$ at a state parameter of zero than the alternatives.

(vii) The parameter, A, (Collins, Pender and Yan, 1992) needed to define the relationship between $(\phi' - \phi_{cv}')$ and state parameter, ξ, was determined to be 0.98. The fit to the experimental data was not strong and would be substantially improved if ϕ' was allowed to be slightly greater than ϕ_{cv}' at a value of state parameter of zero. However such an assumption is theoretically untenable.

(viii) A simpler and slightly better expression was derived for the range of state parameters encountered in the triaxial tests, i.e. ($\phi' - \phi_{cv}'$) degrees = -59.6ξ.

(ix) Bolton's dilatancy index (1986) was found to be proportional to the magnitude of the state parameter, i.e. $I_R = -10.7\xi$. Accordingly, the maximum dilation, expressed in terms of total volumetric strain to total axial strain, was directly related to state parameter by the equation, $D_{B\,max} = -3.2\xi$.

(x) Bolton's dilatancy index was formulated with Q being equal to 9, rather than 10. Bolton had anticipated that lower values of Q might be appropriate for more angular sands.

(xi) Bolton's recommendation of ($\phi'_{max} - \phi'_{cv}$) = $3I_R°$ for triaxial stress state was found to underestimate the difference in shear strength angles by at least 50%. Bolton's equation for plane strain, ($\phi'_{max} - \phi'_{cv}$) = 0.8Ψ, was a better approximation to the triaxial compression data.

(xii) Davis' flow rule (1969) for triaxial conditions, when applied to the experimental data, yielded estimates of dilation angle (ψ_D) which were found to correlate well against both Bolton's dilation index and state parameter. The state parameter correlation was found to be slightly stronger. Dilation angle in degrees can be approximated by multiplying ξ by a factor of –75.

(xiii) The triaxial test data agreed generally with Rowe's (1962) stress-dilatancy expression, and the assumption that ϕ'_f is equal to ϕ'_{cv}.

(xiv) The flow rule of Manzari and Dafalias (1997), which is based on the stress ratio at the onset of dilation, was reasonably supported by the triaxial data for the sand.

From the triaxial test data reviewed in this Chapter, material constants and other parameters have been chosen for the constitutive model of the soil, placed around and above the buried pipe. A constitutive model of the soil is essential to the finite element analysis of the response of the soil-pipe system to external loading. In particular, the critical state shear strength and CSL were chosen, and the relationship linking the difference in effective angle of friction to the state parameter, i.e., ($\phi' - \phi_{cv}'$) radians = $0.98(e^{-\xi} - 1)$, was adopted. Both Bolton's equation for dilation of sand in plane strain and Davis' flow rule were incorporated into the soil model.

The development of the constitutive model is provided in Chapter 6, with validation through comparison of finite element analyses (FEA) with the results of plate bearing tests of the sand contained in a drum. Chapters 7 and 8 subsequently explore the FEA of the the buried pipes in two and three dimensions.

5.7 REFERENCES TO CHAPTER 5

Bishop, A. W. and Green, G. E. (1965). The Influence of End Restraint on the Compression Strength of a Cohesionless Soil. Geotechnique, V15, No. 3, pp 243-266.

Lo, S.-C. R. and Lee, I. K. (1990). Response of Granular Soil along Constant Stress Increment Ratio Path. ASCE, J. of Geotechnical Engineering, V116, No. 3, March, pp 355-376.

Ooi, J.Y. (1990). Bulk Solids Behaviour and Silo Wall Pressures. PhD thesis, University of Sydney, School of Civil and Mining Engineering.

TABLE 5-I. Particle Size Analysis

Particle sizes (mm)			Particle size analysis indices	
D_{10}	D_{30}	D_{60}	C_u	C_c
0.16	0.245	0.41	2.6	0.92

D_n = n % of particles are smaller than this size

C_u = uniformity coefficient

C_c = the coefficient of curvature

TABLE 5-II

Summary of Triaxial Tests

at Set-up (after consolidation, unless stated otherwise)

Test Type	Name	Date	Dimensions before consolidation (mm)	σ'_3 (kPa)	ρ_d (t/m^3)	e_o	I_D (%)
Constant p'	CONP100	9Nov'95	101.2 x 187.7	100	1.610	0.652	65
	CONP102	16Nov'95	101.1 x 187.8	99	1.547	0.719	47
	CONP225	15Nov'95	101.1 x 188.0	224	1.635	0.627	71
	CONP500	11Nov'95	101.2 x 189.2	499	1.634	0.628	71
	CONP500/2	13Nov'95	101.2 x 186.2	500	1.629	0.633	70
Constant volume	DAC001	April'93	101.3 x 188.0	99	1.558	0.707	50
	DAC002	April'93	101.3 x 188.0	147	1.586	0.677	58
	DAC004	Dec'93	101.3 x 188.0	104	1.676	0.587	82
	CVT1/95	22Nov'95	101.1 x 186.3	49	1.533	0.713	48
	CVT2/95	23Nov'95	101.1 x 186.3	49	1.491	0.783	29
CID triaxial	53TRDAC	30Nov'95	101.1 x 186.7	50	1.606	0.656	64
	90TRDAC	7Nov'95	100.9 x 188.7	99*	1.616	0.646	66
	402TRDC	29Nov'95	101.1 x 188.0	400	1.621	0.641	68

* varied between 102 and 88 kPa during the shear stage

TABLE 5-III: Compression Index for the Isotropic Consolidation Stage

Test Name	C	p′ range (kPa)
Constant p′ tests		
CONP100	0.008	43-100
CONP102	0.012	40-100
CONP225	0.011	65-225
CONP500	0.008 0.014	40-148 148-495
CONP500/2	0.009 0.013	35-165 165-500
Constant volume tests		
DAC001	0.007	32-103
DAC002	0.007	40-135
CVT2/95	0.006	18-43
Conventional triaxial tests		
90TRDAC	0.007	47-100
402TRDAC	0.013	100-400

TABLE 5-IV: Secant Modulus Data for the Triaxial Tests

(taken to 0.5q/p′)

Test Name	E_{sec} (MPa)	p′ (kPa)
Constant p′ tests		
CONP100	13.3	101
CONP102	16.6	100
CONP225	28.3	223
CONP500	57.1	499
CONP500/2	49.2	500
Constant volume tests		
DAC001	13.4	101
DAC002	22.7	154
DAC004	26.6	125
CVT1/95	18.5	52
CVT2/95	10.9	47
Conventional triaxial tests		
53TRDAC	11.5	65
90TRDAC	24.6	132
402TRDAC	35.7	531

TABLE 5-V: Strength and Dilation Data

Test	Maxm. Strain $\varepsilon_{a\,max}$ (%)	p'_{max} (kPa)	q/p'_{max}	ϕ'_{max} (°)	Void ratio, e, at:		D_{Tmax}
					q/p'_{max}	$\varepsilon_{a\,max}$	
CONP100	25.8	99.5	1.55	38.1	0.689	0.792	-0.386
CONP102	26.6	100.1	1.48	36.4	0.736	0.806	-0.237
CONP225	26.5	222.7	1.56	38.2	0.654	0.739	-0.310
CONP500	26.3[#]	500.0	1.52	37.4	0.636	0.708	-0.246
CONP500/2	19.9[*]	500.8	1.51	37.2	0.649	0.685	-0.256
DAC001	14.5	304.5	1.41	34.9	0.714	0.723	-0.112
DAC002	26.9	400.5	1.45	35.9	0.683	0.701	-0.100
DAC004	14.4	491.9	1.64	40.1	0.598	0.633	-0.295
CVT1/95	26.3	289.2	1.43	35.3	0.713	0.713	0.000
CVT2/95	26.8	119.9	1.37	34	0.783	0.783	0.000
53TRDAC	27.9	101.4	1.49	36.6	0.690	0.745	-0.373
90TRDAC	24.5	188.9	1.59	38.9	0.665	0.722	-0.367
402TRDAC	26.8	781.8	1.48	36.3	0.640	0.675	-0.197

[#] minor membrane leak
[*] membrane leakage after this strain level

TABLE 5-VI: Estimates of the Critical State Line

Triaxial Test Series	**Γ (intercept at $p' = 1$ kPa)**	**λ (gradient based on ln p')**
Constant volume	1.07	0.055
CID	0.903	0.035
Constant p'	0.99	0.050

TABLE 5-VII: Onset of Dilation Data

Test	**$\varepsilon_{v\ max}$ (%)**	M_c^d	e_c^d	ξ
CONP100	0.16	1.045	0.650	-0.166
CONP102	0.26	1.134	0.715	-0.102
CONP225	0.26	1.084	0.623	-0.149
CONP500	0.54	1.235	0.619	-0.109
CONP500/2	0.41	1.192	0.627	-0.102
53TRDAC	0.20	1.095	0.653	-0.1975
90TRDAC	0.31	1.194	0.641	-0.152
402TRDC	1.03	1.256	0.624	-0.086
DAC001	0.89	1.057	0.703	-0.112
DAC002	0.96	1.156	0.672	-0.121
DAC004	0.35	1.197	0.585	-0.2085

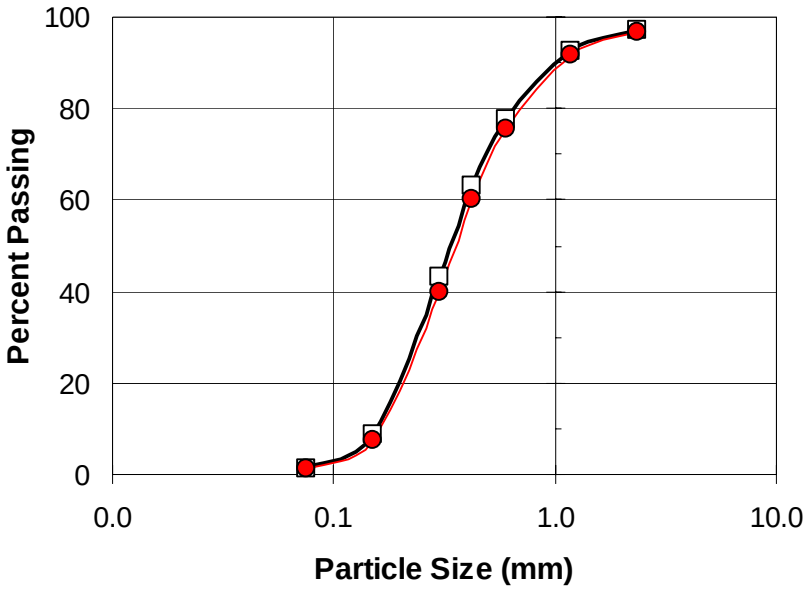

Figure 5-1. Average particle size distributions for two triaxial test specimens (before testing)

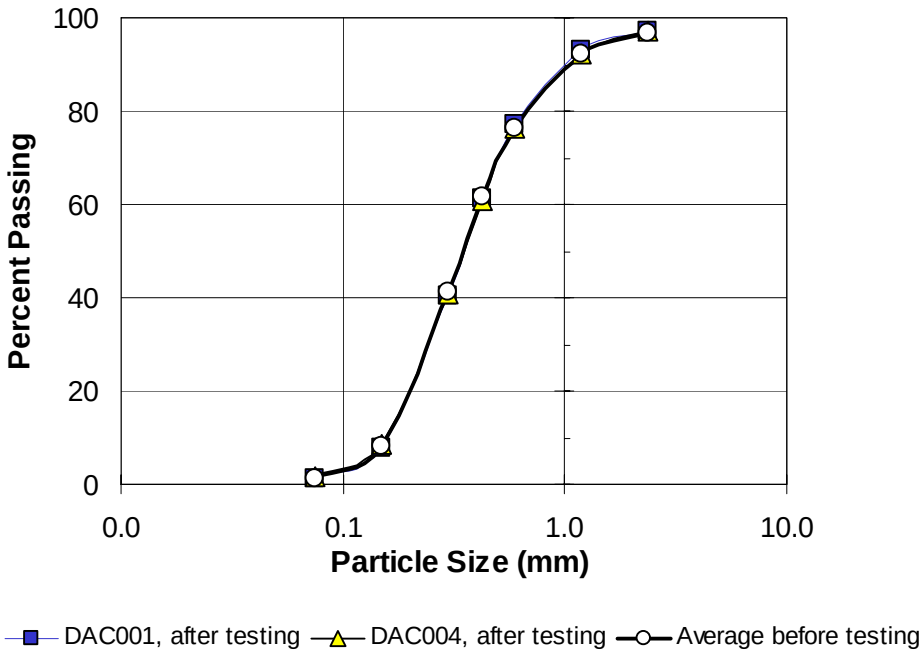

Figure 5-2. Particle size distributions for two triaxial test specimens after testing

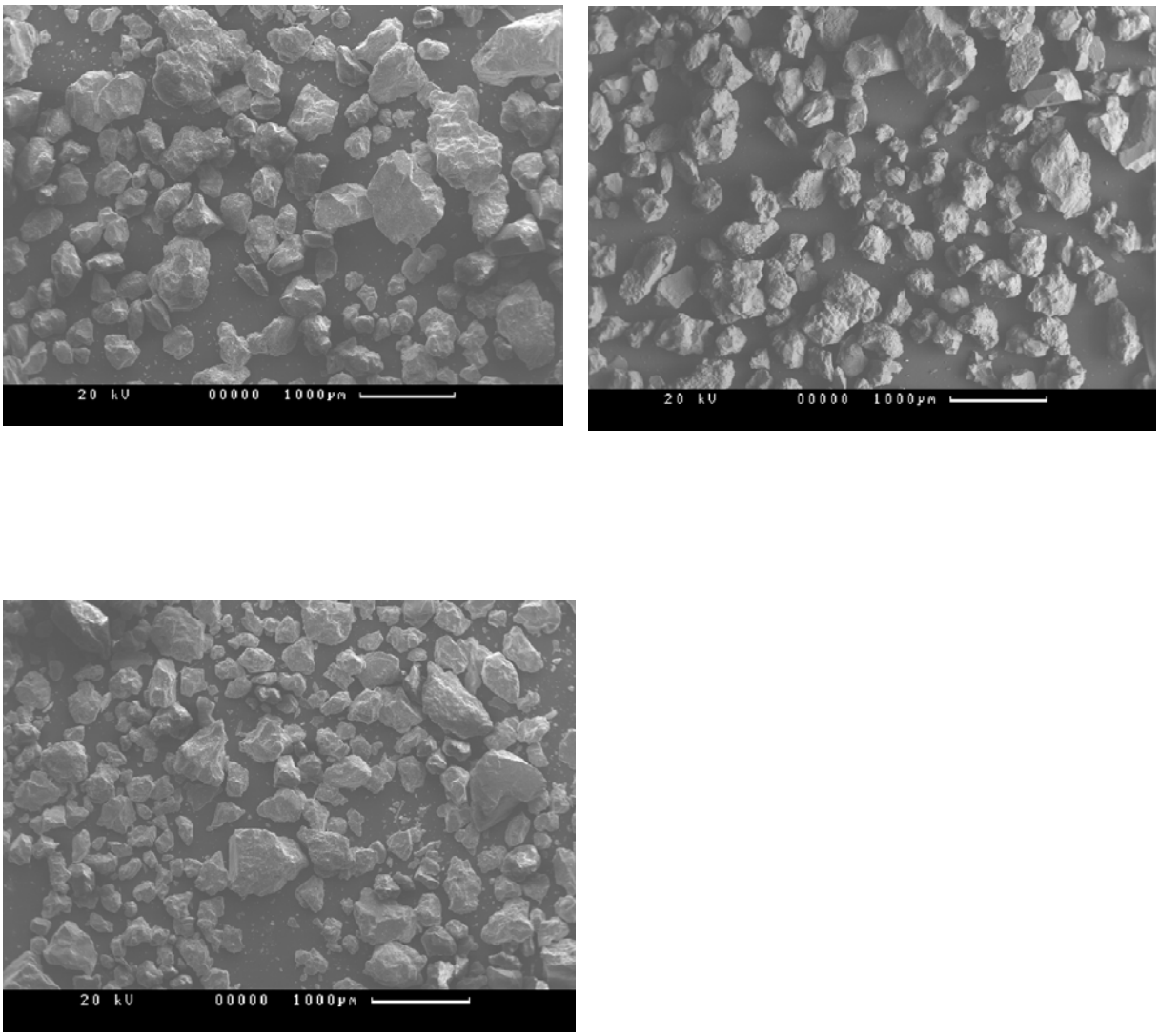

Figure 5-3. Scanning Electron Microscope images of the sand

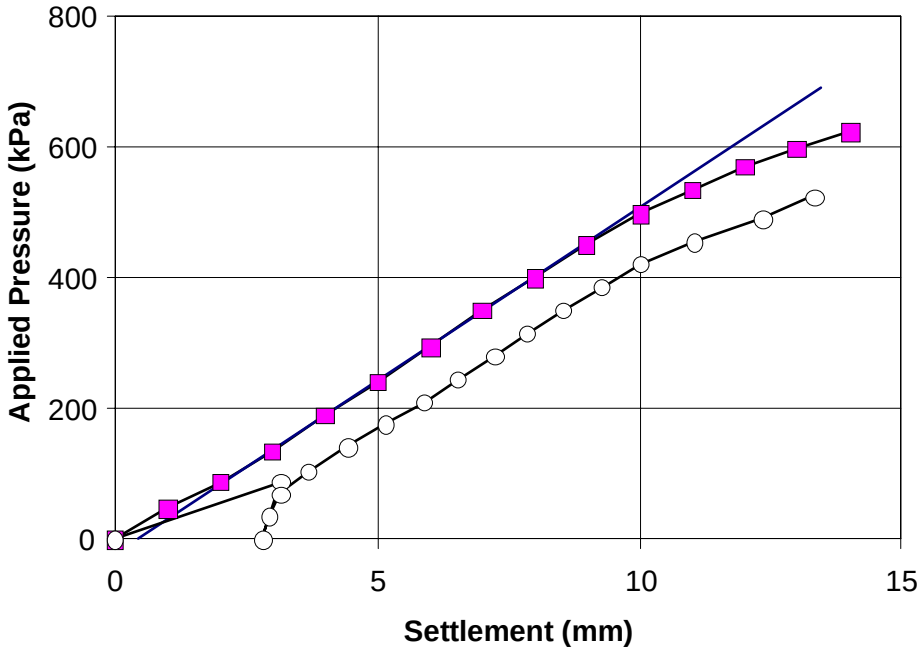

Figure 5-4. Plate loading test results for the sand confined in a drum ($I_D \approx 75\%$)

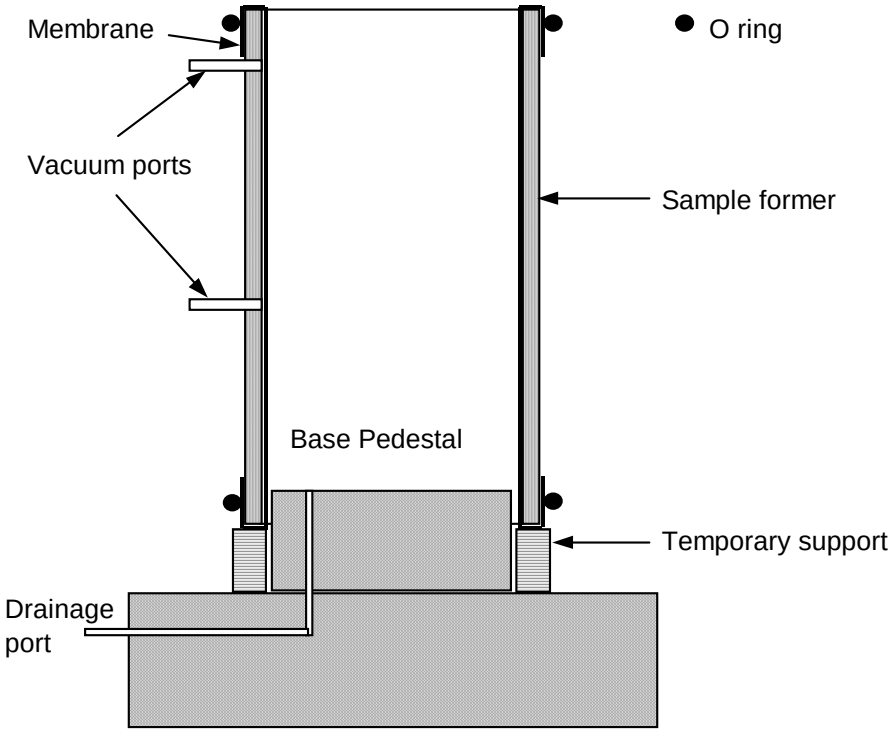

Figure 5-5a. Cross sectional view of sample preparation

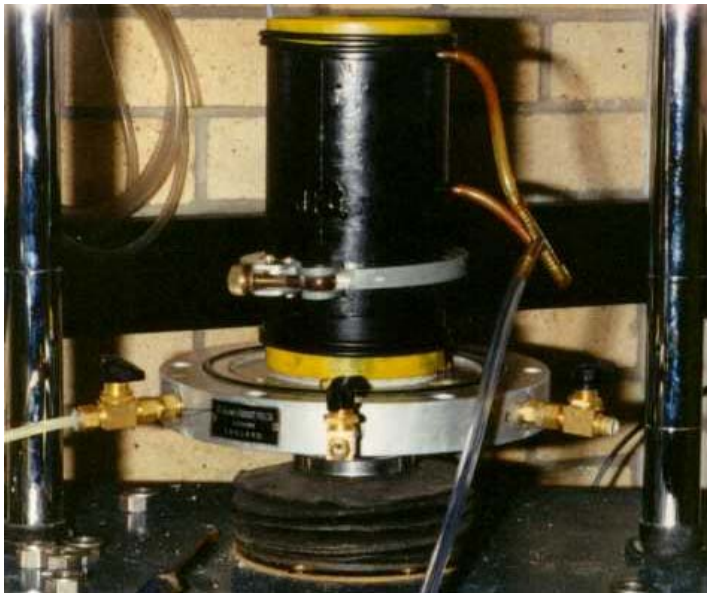

Figure 5-5b. Photograph of the split tube former ready to receive the sand sample

Figure 5-5c. An example of a prepared sample of dry sand

Figure 5-6a. Specimen after a CID triaxial test (90TRDAC, σ_3 = 99 kPa)

Figure 5-6b. Specimen after a constant pressure test (CONP225, p′ = 225 kPa)

Figure 5-6c. Specimen after a constant pressure test (CONP500, p′ = 499 kPa)

Figure 5-6d. Specimen after a constant volume test (CVT2/95)

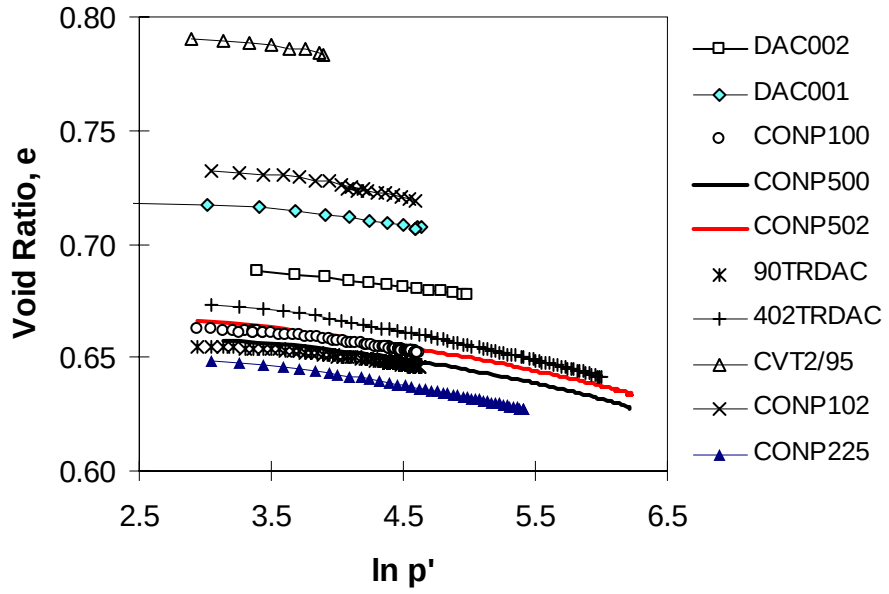

Figure 5-7. Isotropic Consolidation Curves

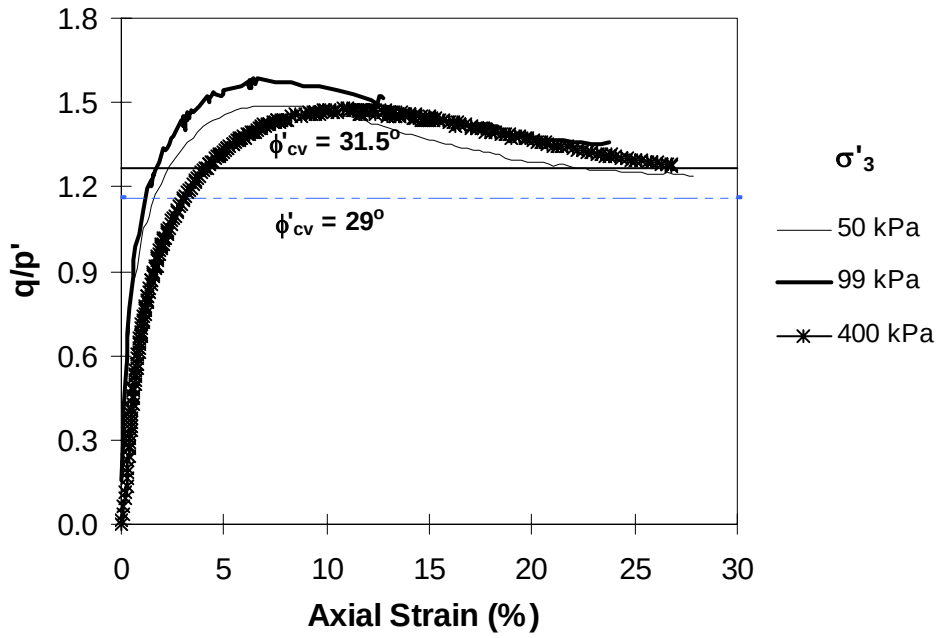

Figure 5-8a. Stress – strain plots for conventional (CID) triaxial tests

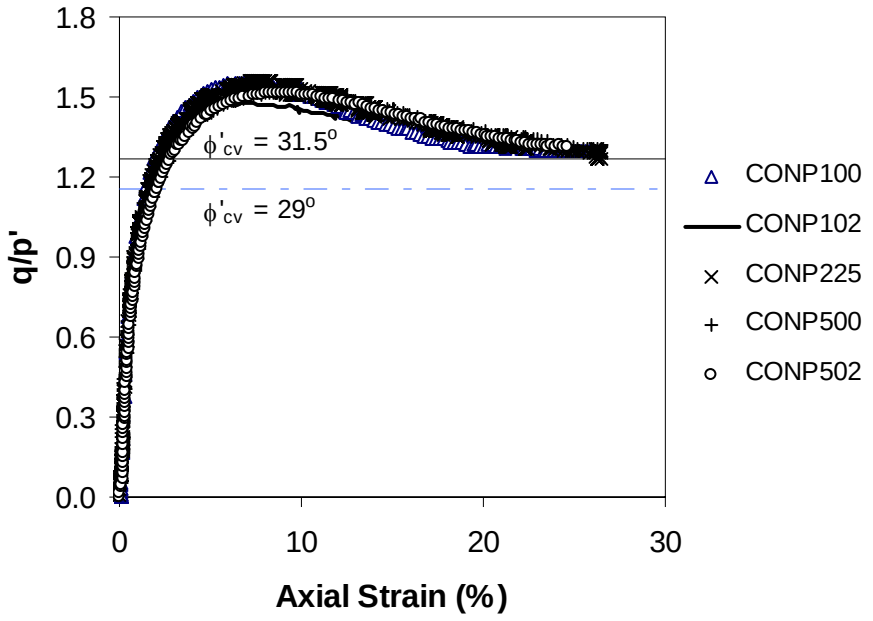

Figure 5-8b. Stress – strain plots for constant mean stress triaxial tests

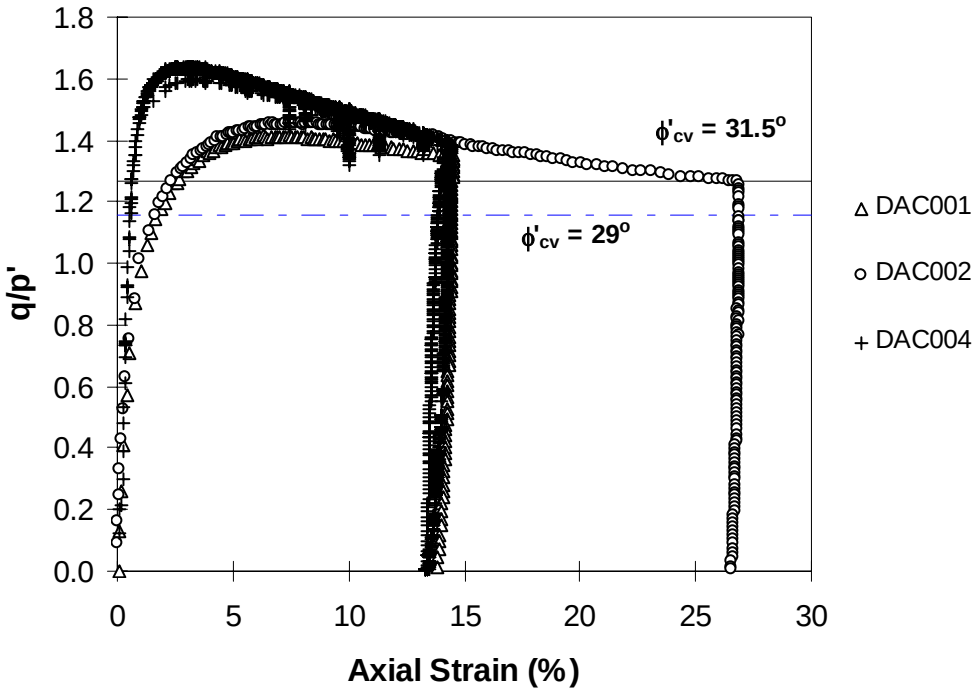

Figure 5-8c. Stress – strain plots for "constant volume" triaxial tests: DAC series

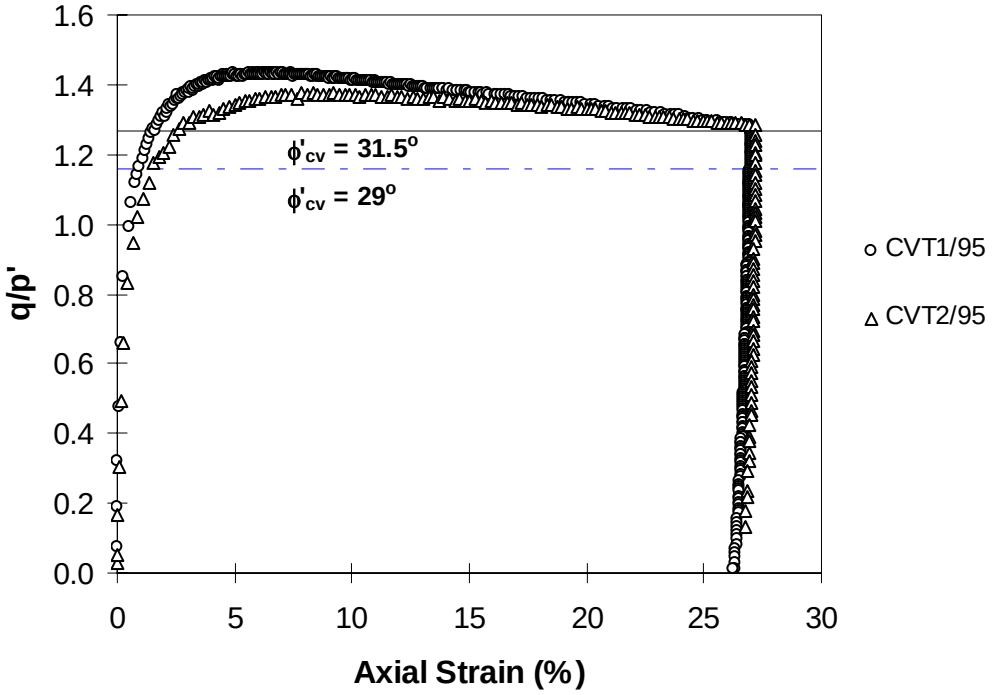

Figure 5-8d. Stress – strain plots for constant volume triaxial tests

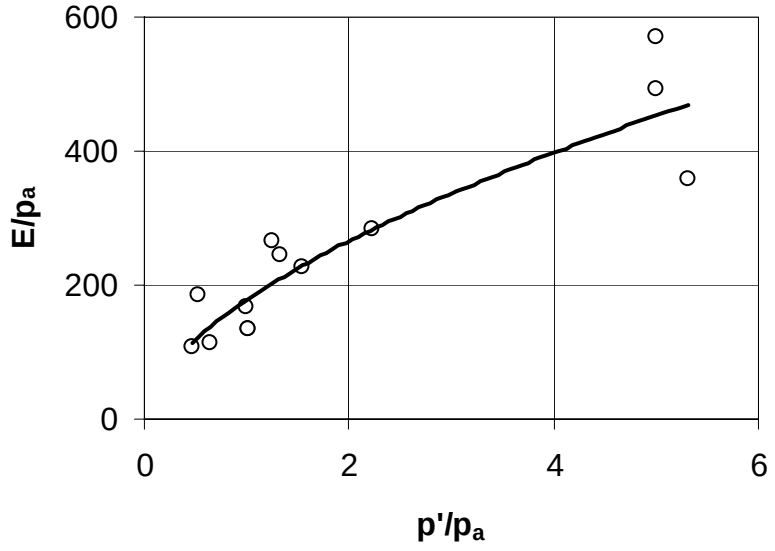

Figure 5-9. Variation of secant modulus at 50% of q/p'_{max} with mean pressure from triaxial test data

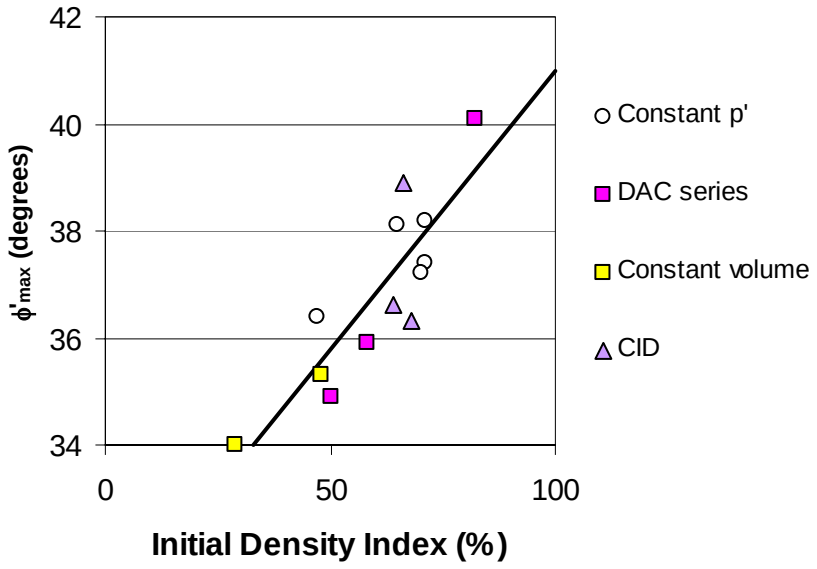

Figure 5-10. Relationship between peak friction angle and initial density index of sample

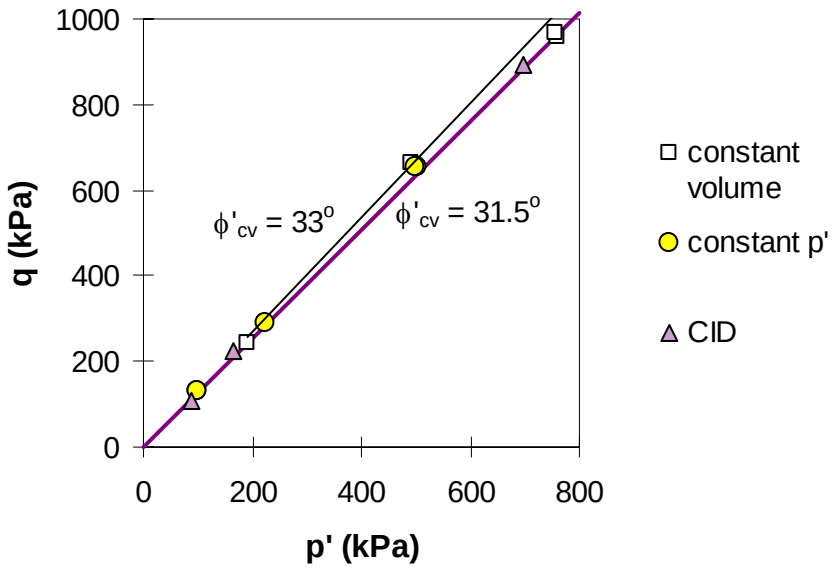

Figure 5-11. Critical state strength (ϕ'_{cv}) estimated from stress state at end of triaxial tests (DAC004 omitted)

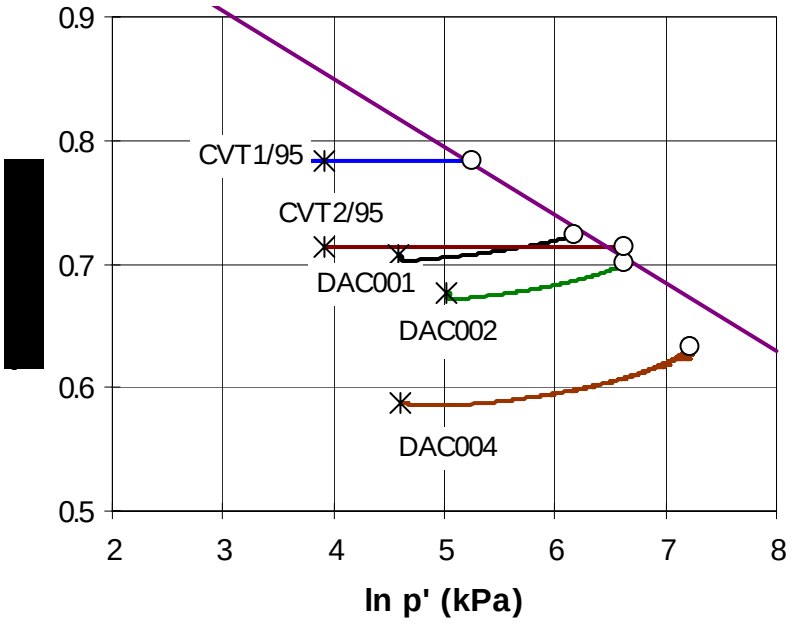

Figure 5-12. Mean stress excursions in the constant volume tests in e – ln p′ space (circles indicate end points of tests)

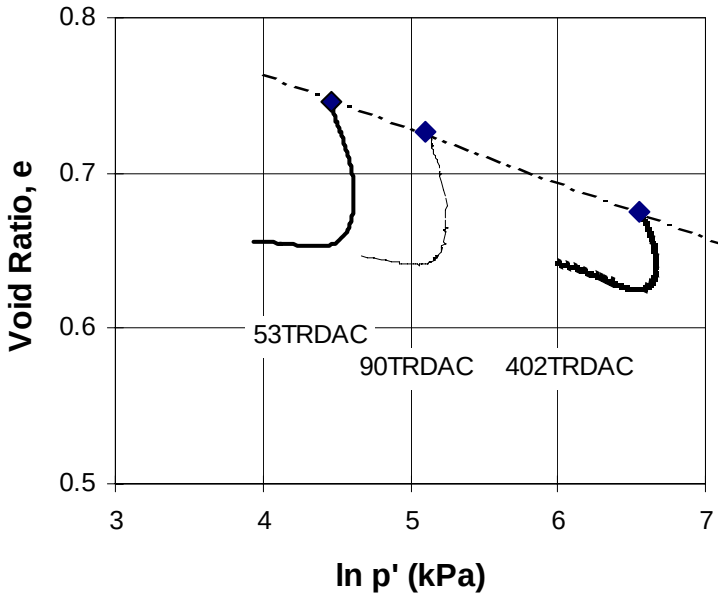

Figure 5-13. Mean stress excursions in the CID triaxial tests in e – ln p′ space

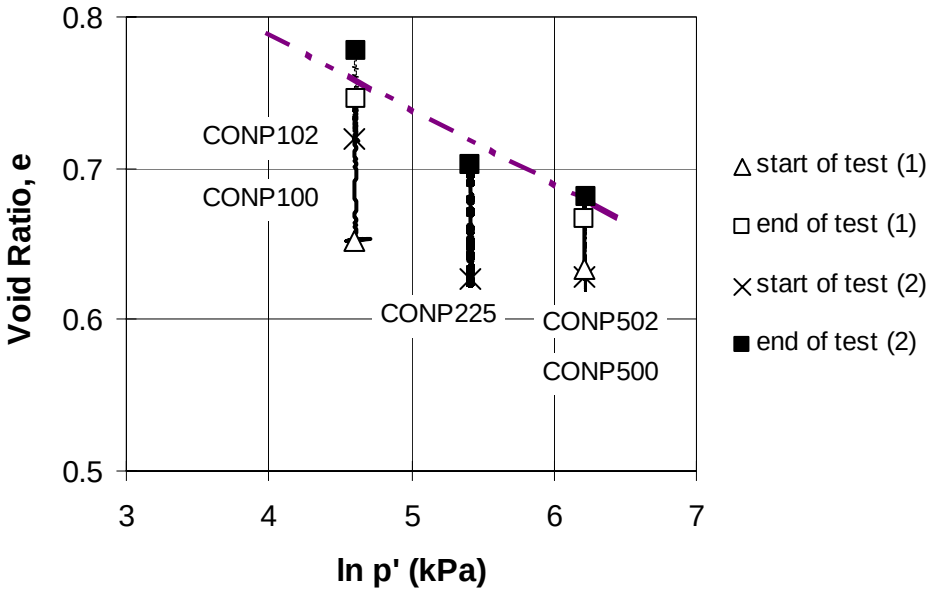

Figure 5-14. Mean stress excursions in the constant mean stress tests in e – ln p′ space

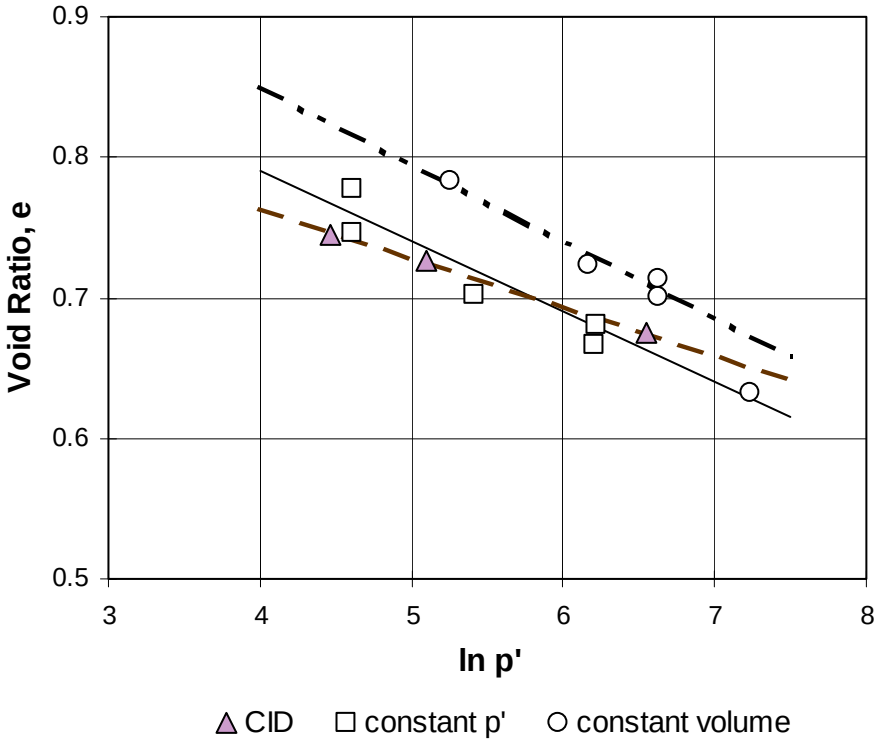

Figure 5-15. Estimates of the CSL for each of the three triaxial test series

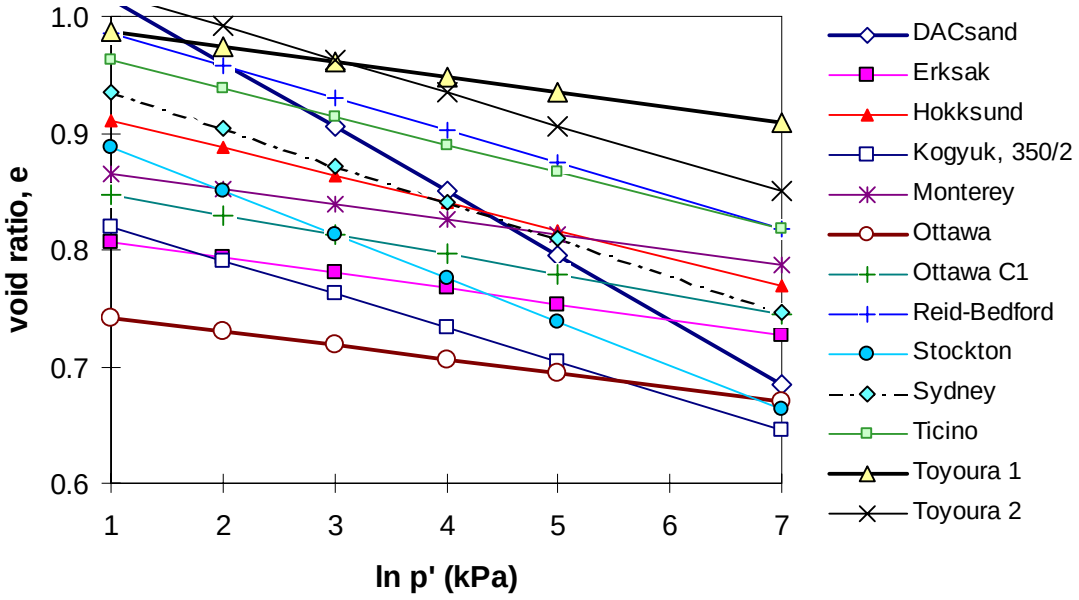

Figure 5-16. Comparison of the CSL for the sand (DAC sand) with other CSL's

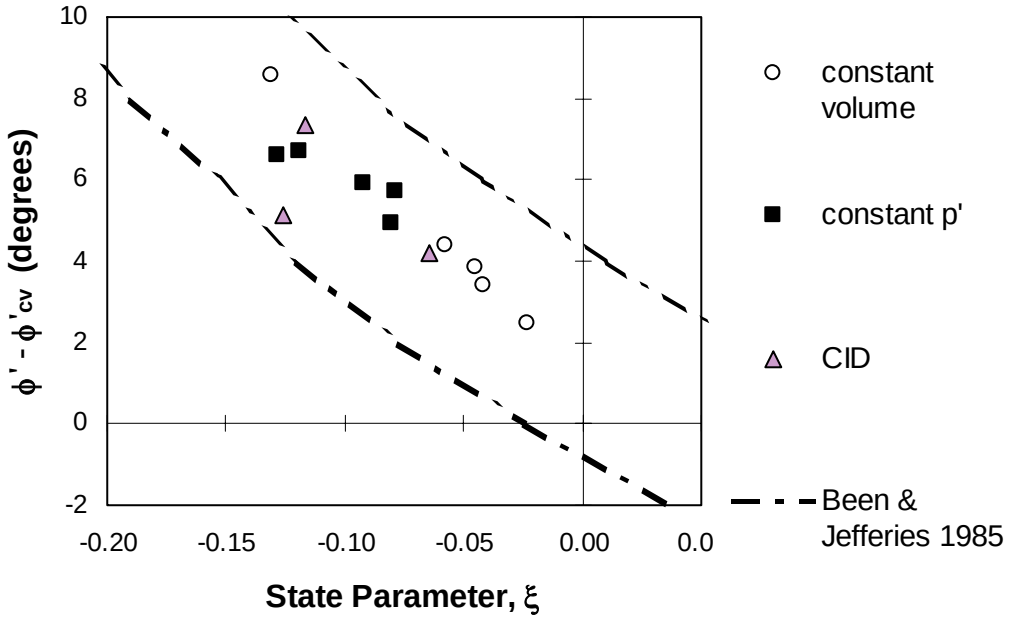

Figure 5-17. ($\phi' - \phi'_{cv}$) in degrees as a function of state parameter, ξ; e_c based on $\Gamma = 1.07$ and $\lambda = -0.055$

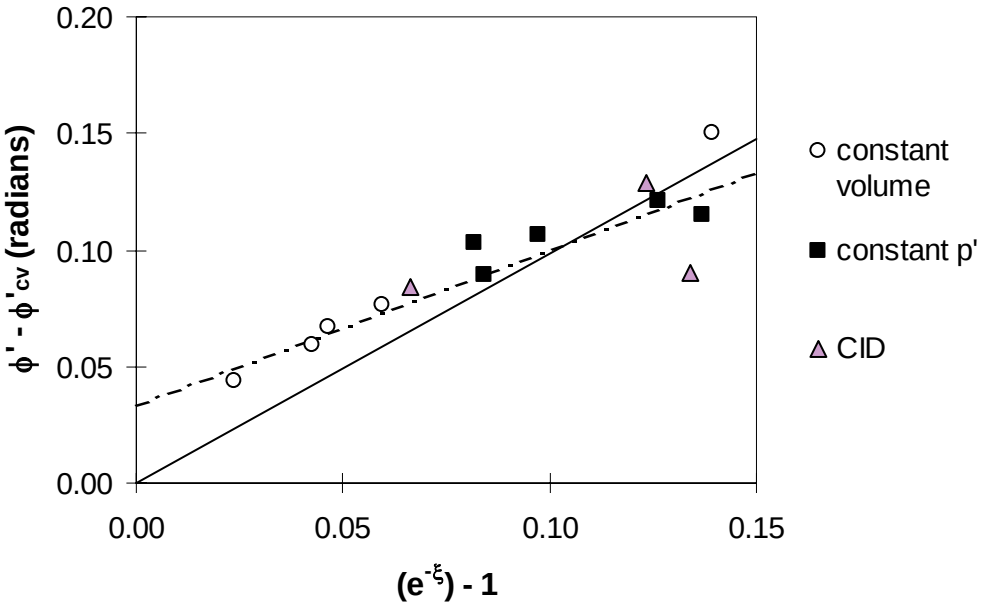

Figure 5-18. ($\phi' - \phi'_{cv}$) in radians as a function of state parameter; data from Figure 5-17 (gradient of line = A = 0.98)

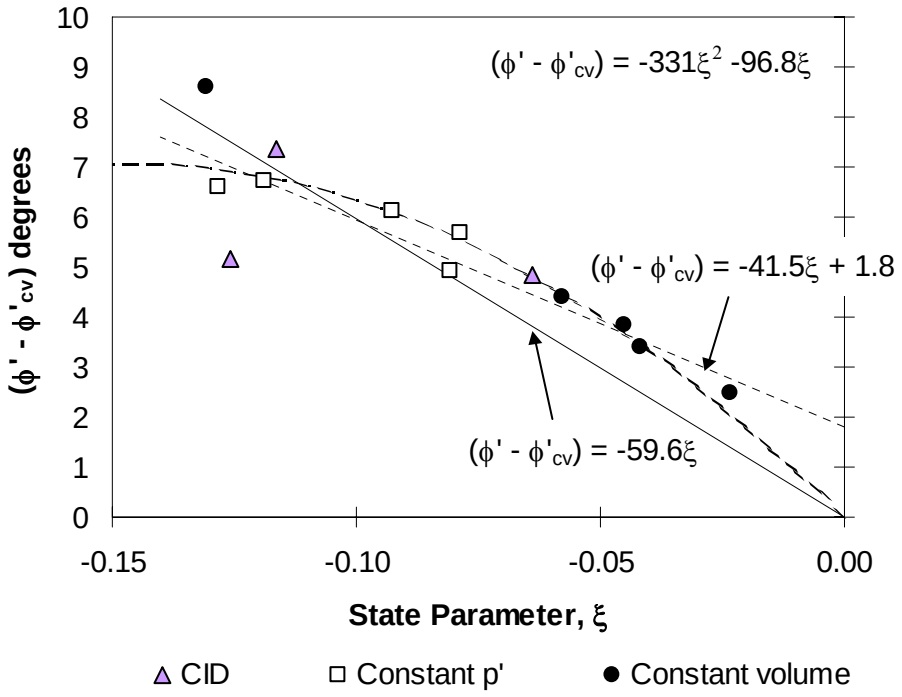

Figure 5-19. Empirical expressions relating ($\phi' - \phi'_{cv}$) to state parameter

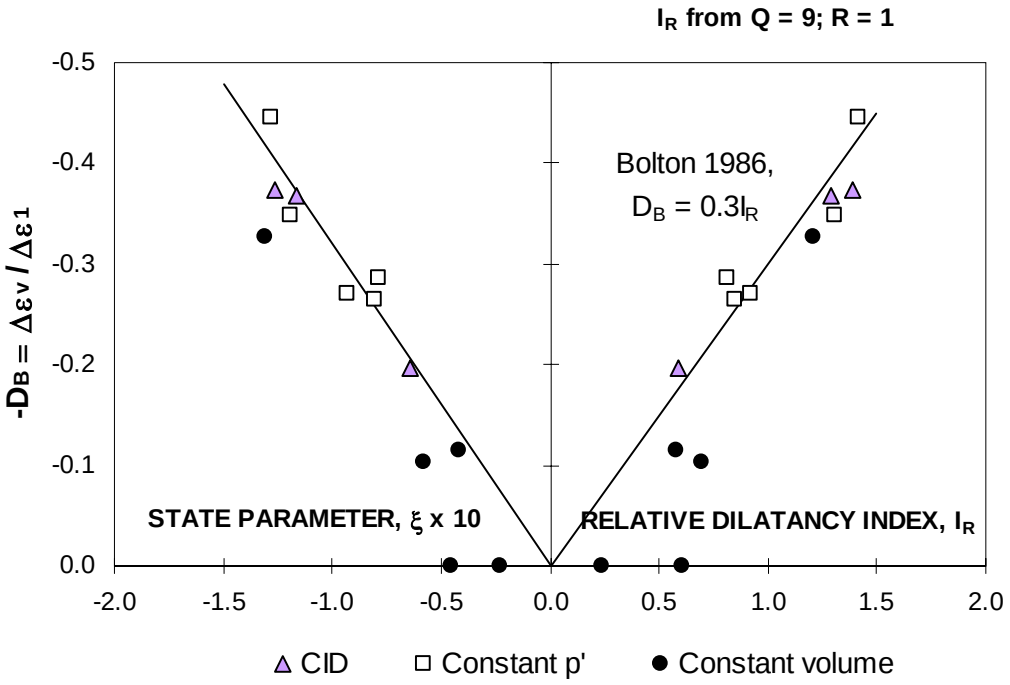

Figure 5-20. Bolton's maximum dilation rate as a function of both dilatancy index and state parameter

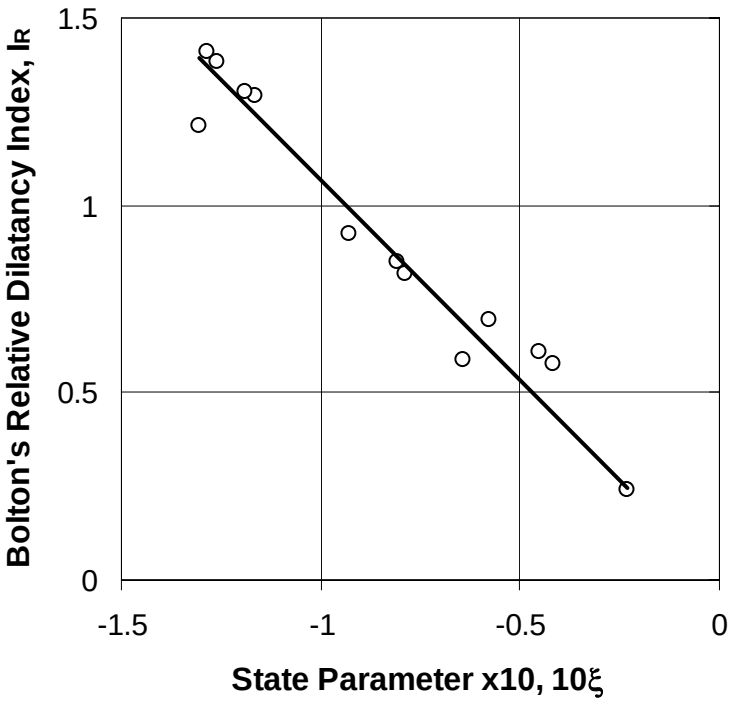

Figure 5-21. Bolton's dilation index as a function of state parameter

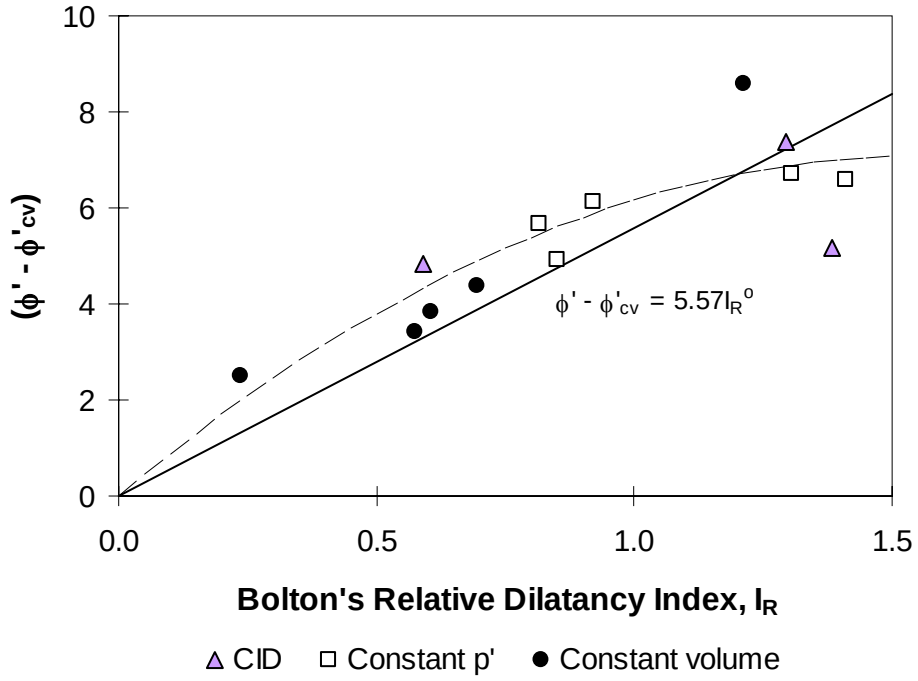

Figure 5-22. Experimental data of ($\phi' - \phi'_{cv}$) plotted against Bolton's dilation index

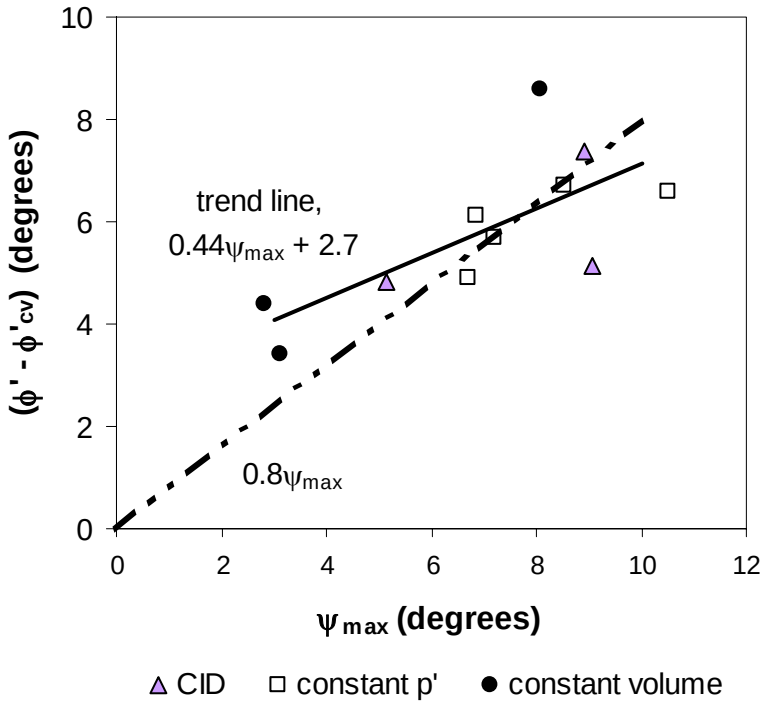

Figure 5-23. Experimental data of ($\phi' - \phi'_{cv}$) plotted against dilation angle estimated from Davis' flow rule (1969)

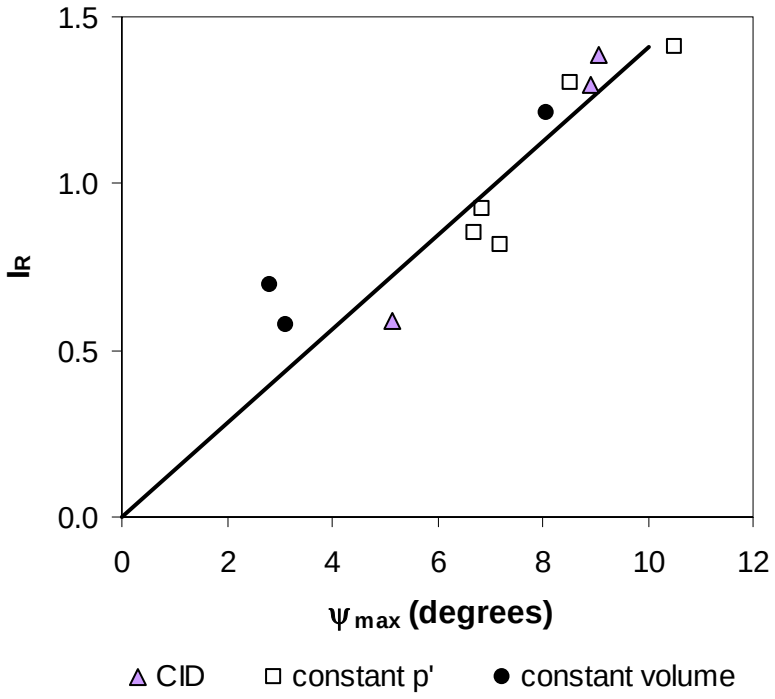

Figure 5-24. Experimental data of Bolton's dilation index plotted against dilation angle, estimated from Davis' flow rule (1969)

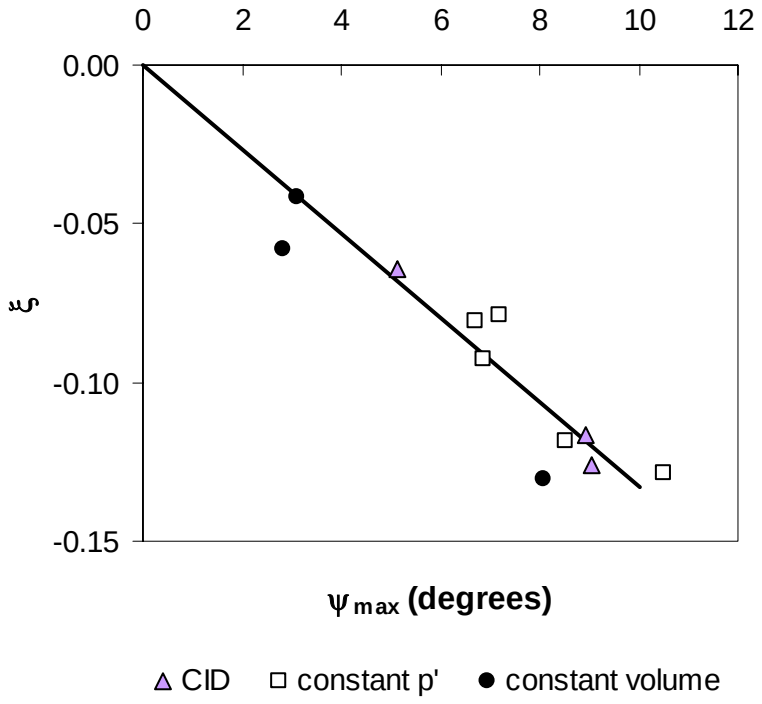

Figure 5-25. State parameter from triaxial tests plotted against dilation angle, estimated from Davis' flow rule (1969)

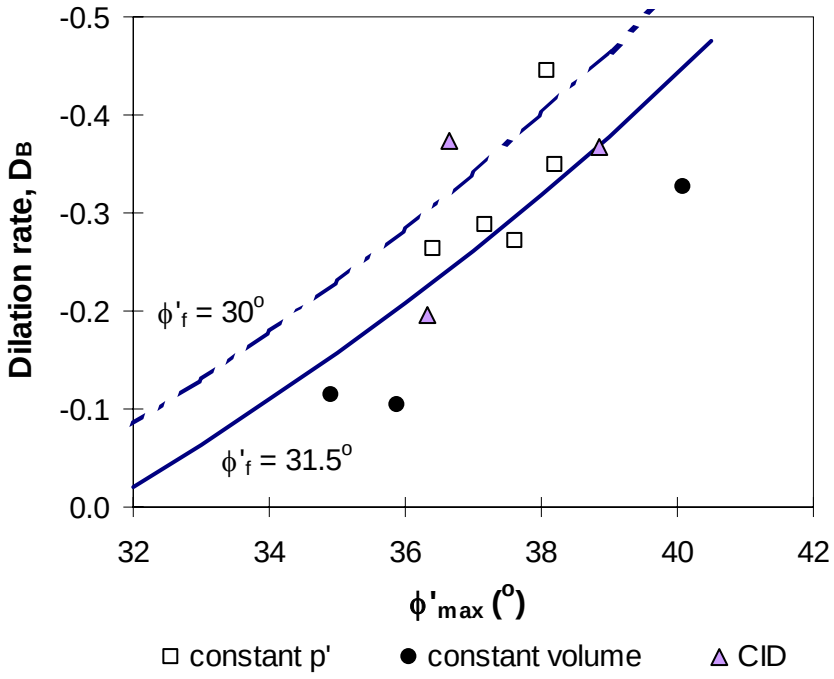

Figure 5-26. Maximum total dilation (volumetric strain to <u>axial</u> strain) against effective peak friction angle

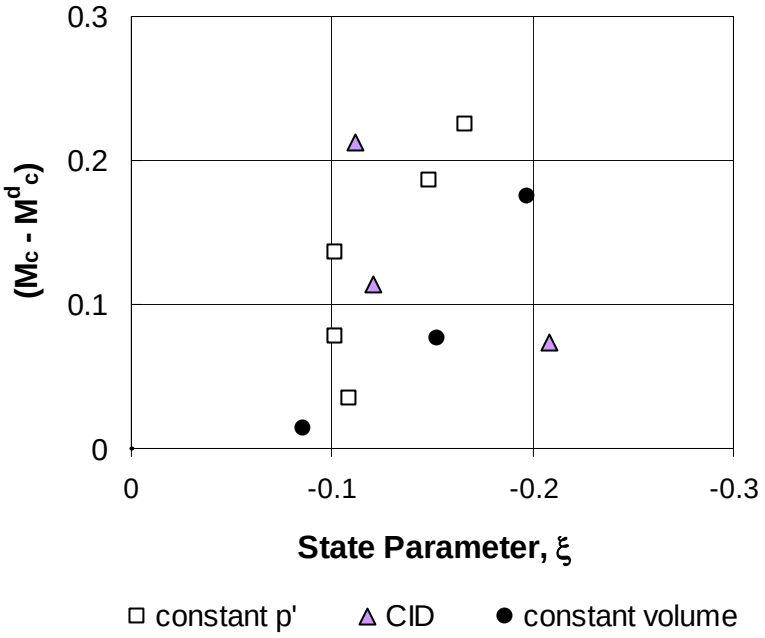

Figure 5-27. $\left(M_c - M_c^d\right)$ against state parameter at the onset of dilation

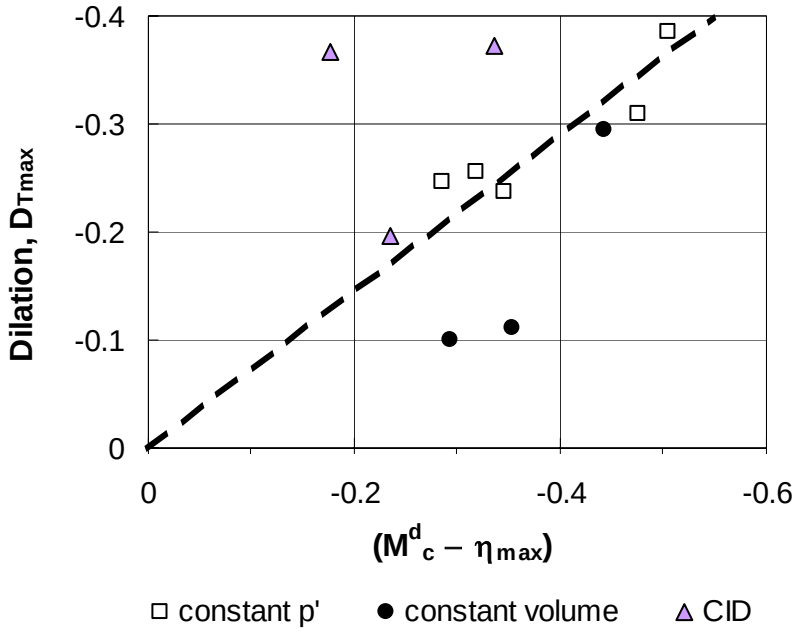

Figure 5-28. Maximum total dilation (volumetric strain to shear strain) against $\left(M_c^d - \eta_{max}\right)$